Emergent Materials
https://doi.org/10.1007/s42247-024-00733-x

ORIGINAL ARTICLE

Effect of SiC addition on laser-based CoNi binary alloy coatings on Ti-6Al-4V alloy

Olanrewaju Seun Adesina[1,2,3] · Abimbola Patricia Popoola[3] · Gabriel Ayokunle Farotade[3] · Babatunde Abiodun Obadele[4] · Olufemi Oluseun Sanyaolu[1,2] · Samson Olaitan Jeje[3] · Azeez Lawan Rominiyi[5]

Received: 15 December 2023 / Accepted: 25 April 2024
© The Author(s) 2024

Abstract

This research explores the impact of variations in laser scanning speed and the incorporation levels of SiC-Ni-Co powders on Ti-6Al-4V alloy using laser surface cladding technique. Key parameters, including a consistent laser power of 700 W, a 4 mm beam spot size, a powder feed rate of 1.0 g/min, and a gas flow rate of 3 L/min, along with fixed powder compositions, were maintained. The laser scanning speeds were adjusted to 0.4 m/min, 0.8 m/min, and 1.2 m/min. Microstructural analyses were carried out using scanning electron microscopy (SEM) while Vickers microhardness was employed to assess coating hardness, and corrosion properties were evaluated using a linear potentiodynamic polarization technique. Following the corrosion attack, the protective oxides formed were identified through SEM and X-ray diffractometer (XRD). The results revealed a strong metallurgical relationship between the clad layer and the substrate, demonstrating the effectiveness of the laser-clad technique. Particularly, the highest laser scan speed exhibited the most significant improvements in hardness and corrosion resistance. The coatings displayed an average hardness value of 1269.20 $HV_{0.1}$, a notable fourfold increase compared to the substrate's value of 334 $HV_{0.1}$. Concerning corrosion, a clear correlation emerged between scan speed and polarization resistance, confirming that higher scan speeds could lead to enhanced polarization resistance.

Keywords Laser surface cladding (LSC) technique · SiC-Ni-Co powders · Microstructure · Corrosion resistance · Ti-6Al-4V

1 Introduction

Titanium and its alloys have been extensively used in engineering fields such as in aerospace structures, heat exchangers and offshore platforms owing to their wide-ranging performances attributed to their low density, good strength-to-weight ratio and corrosion resistance [1–4]. Despite the fact that titanium and its alloys are essential to the aerospace industry due to the aforementioned qualities, widespread non-aerospace (industrial) applications like chemical and offshore or marine systems have been made possible owing to titanium's excellent resistance to many highly corrosive medium, particularly oxide and chloride-rich environment. In addition, to increase the longevity and minimize costs for maintaining the service operations of titanium alloys in industrial applications, surface properties such as reactive environments need to be improved [5]. According to Contu et al [6]. and Oliveira et al [7], the passive behaviour of Ti6Al4V alloy in sulphuric, and hydrochloric acids has been a major concern by many researchers. According

✉ Olanrewaju Seun Adesina
osaadesina@yahoo.com; osaadesina@gmail.com

1 Department of Mechanical Engineering, Redeemer's University, Ede, Nigeria

2 SDG 9, Industry, Innovation and Infrastructure, Redeemer's University, Ede, Nigeria

3 Department of Chemical, Materials and Metallurgical Engineering, Tshwane University of Technology, Pretoria, South Africa

4 Department of Chemical, Materials and Metallurgical Engineering, Botswana International University of Science and Technology, Palapye, Botswana

5 Department of Mechanical and Industrial Engineering, University of Johannesburg, Doornfontein Campus, Johannesburg 2028, South Africa

Published online: 07 May 2024

to Adesina et al [8], a feasible way of extending the range of titanium and its alloys applications is to employ surface modification dynamics. Contu et al [6] explained that when titanium alloy is submerged in sulphuric acid during applications, it is covered by a thin film of TiH_2. According to Tiyyagura et al [9], hydride formation on the surface is usually not stable for lower over-potentials. In order to mitigate this challenge, there is a need to produce a surface that is deficient of such passive film layer. The laser cladding technique has emerged as an innovative solution and promising focal point in addressing challenges associated with inadequate surface properties. This method stands out due to its remarkable ability to generate coatings featuring a dense microstructure, low dilution, a restricted heat-affected zone, and robust metallurgical bonding with the substrates [10]. In addition to the aforementioned properties of laser cladding, processing parameters including laser scanning speed can influence the ideal resulting microstructures and coating qualities. In fact, previous studies in the existing literature have confirmed that the two most important process parameters influencing the geometry and properties of laser cladded coatings are laser power and laser scan speed [11, 12]. For instance, Wang et al [13] investigated the impact of laser scanning speed on the microstructure and characteristics of Fe-based amorphous/nanocrystalline cladding coatings. The outcome showed that as scanning speed progressed, the coating demonstrated the characteristics of greater hardness and improved resistance to corrosion. Tao et al. [14], also investigated the consequences of process factors on the working piece surface roughness during hybrid additive-subtractive manufacturing. The authors reported that with increasing laser scanning speed, the microstructure of the coated layer gradually becomes more refined, and its average microhardness also rises. Yu et al [15] tried to modify the surface of the Ti6Al4V substrate by examining the impact of scanning speed. The outcome showed that due to the molten pool's shorter existence time and lower energy density, higher scanning speeds enhance the coating's microstructure, enhancing its microhardness. Ni-Co alloy coatings, as opposed to Ni coatings or cobalt coatings, exhibit superior corrosion resistance characteristics, according to earlier investigations [16]. As an illustration, nickel slowly degrades in weak acids and becomes passive when a passive oxide coating forms in hostile media, while the superalloys used in gas turbine engines, anti-corrosive alloys, and catalysts for the chemical and petroleum sectors all contain cobalt as an addition [17]. According to Wang et al [18], nickel-cobalt additives have the ability to improve the corrosion resistance of titanium. Adesina et al [17], attempted to investigate the impact of laser scanning speed and the admixed fraction of reinforced Ni-Co powders on clad layer formation and Ti-6Al-4V properties. The research findings revealed that the laser-cladded coatings had improved qualities such as fine microstructure and good metallurgical bonding with the substrate, and inclusion of small holes in relation to the substrate. Adesina et al. [5], further investigated the role of phase composition and microstructure in the corrosion behaviour of laser-based Ti-Co-Ni ternary coatings on Ti6Al4V alloy. It was revealed that the production of dense passive CoO, TiO, TiAl, Ni_2TiO_3, V_2O_5, and Al_2O_3 oxides on the sample surfaces increases the corrosion resistance of cobalt and nickel alloys on titanium.

Limited literature exists concerning the microstructural and corrosion characteristics of ternary coatings applied to Ti6Al4V alloy within a sulfuric environment. Xiong et al. [19], studied laser cladded Ti+SiC coatings on Ti6Al4V, whereas Wang et al [20], focused on investigating the effects of Ni60+Ti_3SiC_2 ceramic additions. Despite their contributions, both studies exhibit constraints regarding the microhardness values acquired and the corrosion behavior of the cladded composite materials. Against this backdrop, this project is designed to address the potential degradation of the titanium alloy's surface when subjected to conditions that could compromise its integrity. The proposed solution involves the application of a SiC-Co-Ni ternary alloy coating using laser cladding methodology. The primary focus of this investigation revolves around the impact of varying laser scanning speeds on the microstructure and mechanical properties of the coated samples. Additionally, the study investigated the electrochemical response of the clad composites through the use of linear potentiodynamic polarization technique. This approach is aimed at comprehensively understanding the corrosion behaviour of the coated samples when exposed to a corrosive environment represented by 1 M H_2SO_4.

2 Experimental

2.1 Materials and process

The substrate (Ti6Al4V) was supplied by TMS Titanium, Poway, California, USA with dimensions (50 * 50 * 5 mm), whose compositions are shown in Table 1. Prior to the laser cladding process and to lessen reflection and enhance laser absorption on titanium alloy, the alloy was sandblasted

Table 1 Elemental composition of Ti6Al4V

Ti	Al	V	Fe	C	O	N
Bal.	6.16	4.01	0.11	0.007	0.10	0.005

جامعة قطر QATAR UNIVERSITY

with silica grit sand and cleaned with acetone to remove any contaminant. The morphology in terms of SEM and EDS is shown in Fig. 1a and b respectively. Titanium is clearly identified as the predominant constituent, verifying its purity (depicted in Fig. 1b). In Fig. 1a, the alloy displays a distinct surface texture marked by dispersed, diminutive black pits and an overall grayish surface etching. As detailed by Liu et al. [21], the material structure encompasses both alpha and beta (α+β) phases. The grey α phase, possesses a hexagonal close-packed (HCP) crystal structure, while the β phase exhibits a body-centered cubic (BCC) crystal structure, presenting as a darker component. The α phase is stabilized by aluminum (Al), while the β phase is upheld by Vanadium (V) [22, 23].

For the cladding process, silicon carbide, cobalt, and nickel powders, each with a purity level of 99.9 percent and an average particle size ranging from 45 to 95 microns, were applied onto the substrate Ti6Al4V alloy. The SEM micrographs of the SiC, Co, and Ni powders are shown in Fig. 2a-c. In the pursuit of optimal consistency, a mixture comprising 60% SiC, 20% Co, and 20% Ni powders underwent thorough premixing and homogenization within a Turbula T2F shaker mixer at a rotational speed of 49 rpm for a duration of 8 hours. This meticulous procedure was undertaken to heighten homogeneity and flow characteristics, thus averting any potential for nonuniform amalgamation due to powder agglomeration, which could lead to irregular powder flow behaviour.

2.2 Processing of laser-clad surfaces

A Rofin Sinar DY044 Continuous Wave Nd: YAG laser system, with a power output of 4.4 KW, and featuring a KUKA articulated arm robotic system, was employed for the cladding process. This involved applying a composite mixture of 60SiC-20Co-20Ni powders onto the Ti-6Al-4V alloy. These particles were included by adding them to the molten pool that the laser beam had formed as it scanned

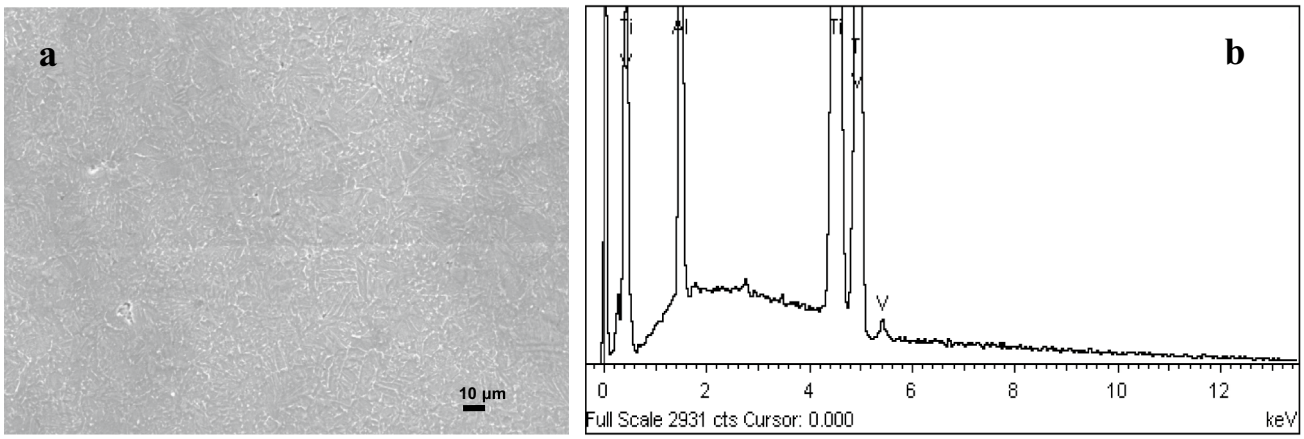

Fig. 1 Morphology of Ti6Al4V in terms of (**a**) SEM and (**b**) EDS

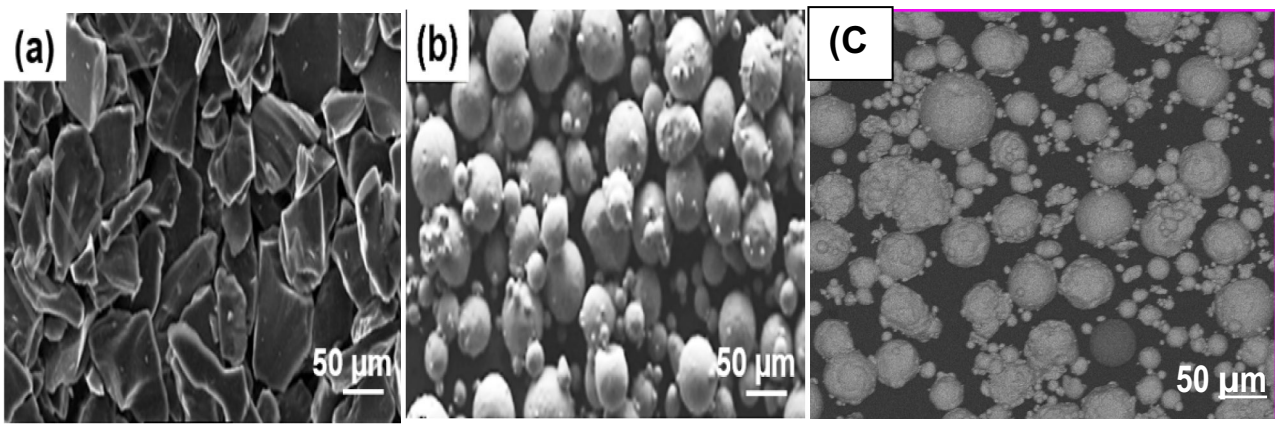

Fig. 2 SEM micrograph of (**a**) SiC (**b**) Co (**c**) Ni powder

over the substrate. The laser's processing parameters were set to its optimal values of 700 W of laser power, 1 g/min of gas flow, 4 mm of beam spot size, and 0.4, 0.8, and 1.2 m/min of scan speed. In addition, previous studies established the limitations of titanium and its alloy as regards the poor thermal conductivity (17 W/MK), which is less than that of steel 40 (W/MK), and these limitations could result in contraction or thermal deformation of the alloy when energy intensity is high [24]. In addition, it is stated that when the energy density is too high for titanium alloys, it results in a larger band of HAZ, which alters the properties of laser cladding techniques as regards low dilution [25]. On the other hand, a lower laser power can effect a limitation of improper powder melting. Zhang et al [26], stated that less power could also cause incomplete mixing in the molten pool, resulting in poor metallurgical bonding or adhesion. In view of the aforementioned, the selection of the best laser processing parameters was considered.

Numerous clad tracks were deposited with 50% overlap at a 45° angle to the substrate to provide coatings with a wide surface area. During deposition, argon gas at a flow rate of 3 L/min was employed to establish a non-oxidizing environment around the molten pool to prevent oxidation, given that titanium has a strong affinity for oxygenated environment. The laser cladding parameters used to produce 60SiC-20Co-20Ni coatings on Ti-6Al-4V alloy are listed in Table 2. Figure 3 represents the cladded samples at laser speed of 0.4, 0.8, and 1.2 designated with sample I, J, and K respectively.

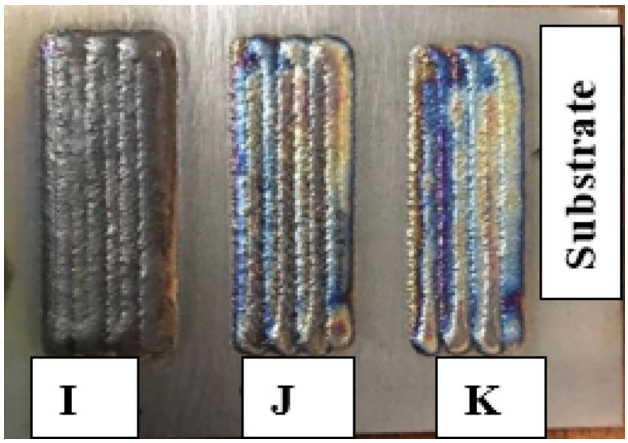

Fig. 3 As-cladded 60SiC-20Co-20Ni samples at different speed on Ti6Al4V alloy

2.3 Characterization of produced laser-cladded samples

For the laser cladding procedure, the coatings intended for microstructural assessment underwent a grinding regimen utilizing SiC grinding papers with grit sizes of P80, P320, P1200, and P4000. This grinding was executed using a Struers TegraForce-25 unit, which incorporated an automated diamond suspension dispenser. Following the grinding phase, the cladded samples were subjected to a polishing process. Initial polishing was performed on an MD-Largo platform, followed by a refining step utilizing an MD-Chem OP-S polishing cloth combined with Diapro diamond suspension. Subsequent to polishing, the prepared cladded samples were subjected to etching using Kroll's reagent (composed of 92 ml H_2O, 6 ml HNO_3, and 2 ml HF). The etching duration was approximately 10 s, and its purpose was to attain distinct and precise visibility of the microstructural phases present within the samples.

The morphologies of the laser-clad coatings were studied using a FE-SEM JSM-7600F scanning electron microscope (SEM), and the compositions of the elements were determined using energy dispersive spectroscopy (EDS). Intermetallic compounds were identified using a Philips PW1713 X-ray diffractometer (XRD) with monochromatic Cu-K radiation set at 40Kv and 20mA, while phase identification was performed using the Philips Analytical X'Pert High Scores program in conjunction with an internal (ICSD) database. The step size is 0.02° and the scan ranges from 10 to 80 degrees at 2 theta.

2.4 Hardness examination

The assessment of micro-hardness profiles for the cladded samples (both coating and substrate regions) was carried out employing the EMCOTEST Vickers Hardness Tester. The goal of this investigation was to clarify how heat input and cooling affected the material characteristics in the various locations. Vickers hardness profile measurements were obtained with a bearing load of 100 gf (0.98 N) and a 10 s dwell time on the cladded area's surface adjacent to the

Table 2 Laser processing parameters used for the deposition of 60SiC-20Co-20Ni coatings on Ti-6Al-4V substrate alloy

Sample	Coating	Power (W)	Laser scan speed (m/min)	Beam diameter (mm)	Powder feed rate (g/min)	Gas flow (L/min)
I	60SiC-20Co-20Ni	700	0.4	4	1.0	3
J	60SiC-20Co-20Ni	700	0.8	4	1.0	3
K	60SiC-20Co-20Ni	700	1.2	4	1.0	3

substrate. Following this, the average hardness value was calculated for each coating, derived from five separate indentations made in close proximity on the 60SiC-20Co-20Ni cladded surface. This procedure was performed throughout the longitudinal axis of every single sample as well as on the coating's exposed surface.

2.5 Electrochemical test

Samples designated for corrosion study were cut into dimensions of 1 x 1 x 1 cm. Subsequently, an insulated copper wire was affixed to one surface and secured with aluminum tape. The prepared specimen was then positioned within a rubber mold, and a mixture of epoxy resin and catalyst was poured into the mold. After the cold mounting process, the specimen underwent grinding using 1200 grit SiC paper and was further polished with a 3 mm finish diamond suspension. Following this, the specimens underwent ultrasonic cleaning in ethanol before immersion in a 1 M H_2SO_4 acid solution to assess corrosion. Employing a three-electrode corrosion cell setup, the experiments utilized a saturated silver/silver chloride electrode (Ag/AgCl) as the reference electrode, a graphite rod as the counter electrode, and the sample as the working electrode. Electrochemical experiments were conducted at room temperature using a computer driven Autolab potentiostat (PGSTAT302N) equipment connected to a computer system. The in-built software, General-Purpose Electrochemical Software (GPES) version 4.9 was employed to analyze the Tafel region and determine the electrochemical data; corrosion potential (E_{corr}), polarisation resistance (Rp) and corrosion current (I_{corr}). The potentiodynamic polarization curves were generated with a scan range from -2.0 to 1.5 V and a scan rate of 2 mV/s. Prior to the potentiodynamic polarization scan, the specimens were cathodically polarized at -1000 mV for 5 minutes, followed by an open circuit potential measurement for approximately 60 minutes. To ensure repeatability, all tests were conducted in triplicate.

3 Result and discussions

3.1 Morphology analysis of 60SiC-20Co-20Ni coatings on Ti6Al4V

The SEM images of 60SiC-20Co-20Ni coatings deposited on Ti-6Al-4V substrates at laser scan speeds of 0.4, 0.8 and 1.2 m/min are shown in Fig. 4. The overall development of the microstructure is governed by the relationship between the thermal field created during the laser-material interaction and the crystal growth mechanism. This relationship accounts for the differences in morphology observed at different laser scan speeds. At a laser scanning speed of 0.4 m/min (depicted in Fig. 4a), the microstructure displays the presence of three distinct phases. Notably, there are light secondary precipitates, primary eutectics with a gray hue, and darker precipitates situated along the grain boundaries. The dark precipitates along the grain boundaries signify zones enriched in carbon. At such low speed of material deposition, there is sufficient laser-material interaction time, leading to partial melting of hard SiC particles, and form a segregation of carbon-rich phases within the solidifying phase. This carbon enrichment arises due to the diffusion of carbon resulting from the dissociation mechanism of SiC. As a consequence of this dissociation, diverse carbon-containing phases form, each possessing differing degrees of carbon solubility.

Within the melt pool, the carbon content increases, leading to the creation of carbon-rich compounds that remain meta-stable as the solidification process unfolds. The prevalence of the light precipitates could be attributed to the substantial energy imparted by the laser source. This high-energy input facilitates the dissociation of SiC compounds, enables the kinetic transport of Si, C, Ni, and Co atoms, and contributes to the enthalpy-driven formation of new phases.

Figure 4b shows the SEM micrograph of 60SiC-20Co-20Ni coatings fabricated on Ti-6Al-4V alloy at a laser scan

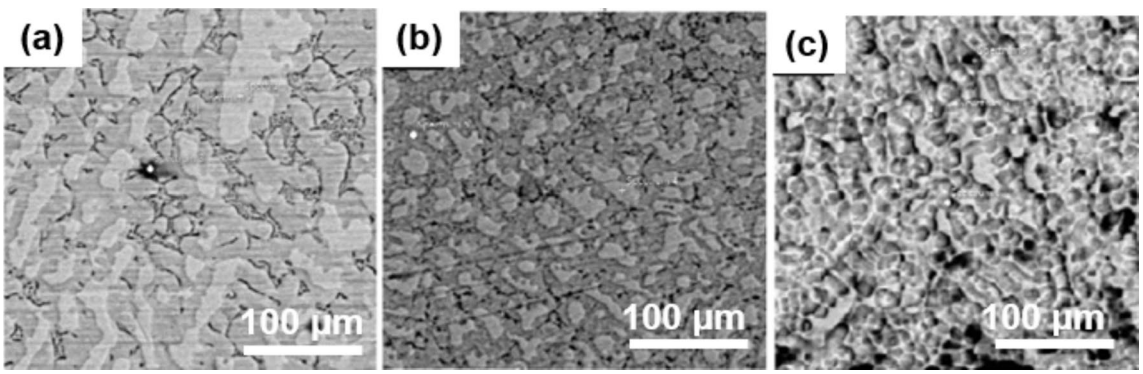

Fig. 4 Morphology of clad sample at laser scan speed of (**a**) 0.4 m/min (**b**) 0.8 m/min (**c**) 1.2 m/min

speed of 0.8 m/min. With reference to Fig. 4a, b displays smaller grains and larger proportions of dark and grey precipitates. Increased laser scan speed leads to reduced laser-material interaction time and increased solidification rate. Consequently, smaller grains are formed due to insufficient time for grain growth (Light-coloured precipitates appear smaller).

Figure 4c shows a different morphology compared to Fig. 4a and b. The microstructure is characterized by equiaxed, or globular grains discerned as the appearance of titanium and carbon-rich zone. Dey et al [27], observed equiaxed grains in a study that employed B_4C and SiC as precursor on Ti-6Al-4V alloy by laser cladding and was found to be enriched with titanium and carbon. A rationale behind the formation of this feature is the fragmentation of the secondary dendrite arms during solidification [28]. The generation of equiaxed grains can also be attributed to both grain detachment and heterogeneous nucleation due to the flow in the molten pool at higher scan speed [29]. However, according to Luo et al [30], the equiaxed or globular microstructure has a superior balance of strength and ductility.

The resultant effect of varying scan speeds can be inferred from the SEM micrographs. There is a transition from plate-like grains to globular equiaxed grains with increasing scan speed. When the laser scan speed increased, due to the reduced laser-material interaction time, there is a reduction in the laser energy input to the melt pool and corresponding decrease in heat accumulation within the pool. This increases the cooling rate of the melt pool, and influences the size and shape of the crystal grains, refining the grains from columnar structure to globular patterns [31].

3.2 Intermetallic regions

Figure 5a, b and c represent the microstructure of the intermetallic regions between the substrate and the coatings of the cladded sample at scan speed of 0.4, 0.8, and 1.2 m/min. As observed, the morphologies of the samples comprise clad zone (Coating), transition zone (interfacial zone and Heat affected zone), and base material (Substrate). Due to variation in laser scan speed and corresponding solidification rates, different features were revealed within the microstructure of the laser-assisted cladded coatings [32]. It is observed that the interfacial zone showed distinct band width, which can be attributed to the increasing ultra-chilling effect as laser scanning speed increases. The SEM micrographs revealed a refinement in grain of the coatings up to the level of a globular grains as the laser scanning speed increases (Fig. 5b and c). This is owed to the presence of carbon-rich zone represented by dark precipitates along the grain boundaries. As carbon diffuses from the dissociation mechanism of SiC, the carbon content within the melt-pool increases with increasing scanning speed and forms enriched carbon compounds that are meta-stable as solidification proceeds. This can be linked to the laser-material interaction period, as laser scan speed of 1.2 m/min resulted to a reduced laser-material interaction period, higher cooling rate and increased nucleation rate with corresponding formation of smaller grains within the coatings, after the solidification process. The presence of carbon-rich zones often correlates with the formation of carbides, which can contribute to increased hardness in the coating. Also, the precipitation of carbide phases may act as barriers against corrosive elements, contributing to the overall corrosion resistance of the coated substrate. Furthermore, in line with the work of Qin et al [33] and Chen et al [16], the thinner heat affected zone band width observed in this study can be as a result of the thinner layer of the substrate melted with limited penetration of Co-Ni atoms into the surface layer of substrate. The equiaxed-shaped microstructure in Fig. 5c is enriched with titanium and carbon [27] and can be owed to the solidification rate as the melt pool cools rapidly with higher laser scanning speed. Further observations revealed that there were no pores at the interfacial zone of sample I, J, and K. this means that the thermal stress induced by the laser within the material had no effect on the zone regardless of the laser scan speed.

3.3 Microhardness analysis

Different combinations of laser scanning speed during laser processing were used to measure the microhardness of the substrate and coatings. As depicted in Fig. 6, the microhardness values of 60SiC-20Co-20Ni coatings displayed higher values with respect to the hardness of the substrate which has a value of 345.2 $HV_{0.1}$. The hard nature of the SiC-Co-Ni admixed compound of the coatings could be responsible for the increase in microhardness of the samples. Dey et al. [27], reported an increase in hardness of Ti6Al4V substrate when coated with B_4C and SiC using laser technique. Sample K, processed at a scanning speed of 1.2 m/min, yielded the most robust coating with a remarkable increase of 105.14% in hardness compared to the substrate's hardness. The globular grains formed at higher laser scanning speeds, are key contributors to the enhanced hardness. Smaller grain sizes, as seen in the coatings processed at higher scanning speeds, are associated with increased hardness due to a higher volume fraction of grain boundaries, which act as barriers to dislocation movement, thereby resisting plastic deformation. The microhardness enhancement, especially in the sample processed at a scanning speed of 1.2 m/min, can be attributed to the rapid solidification rates. The use of 1.2 m/min laser scanning speed influences the microstructural integrity and fosters a stronger metallurgical bond between the coating and substrate. According to Baicheng [26], Wang et al. [34] and Hainsworth et al. [35],

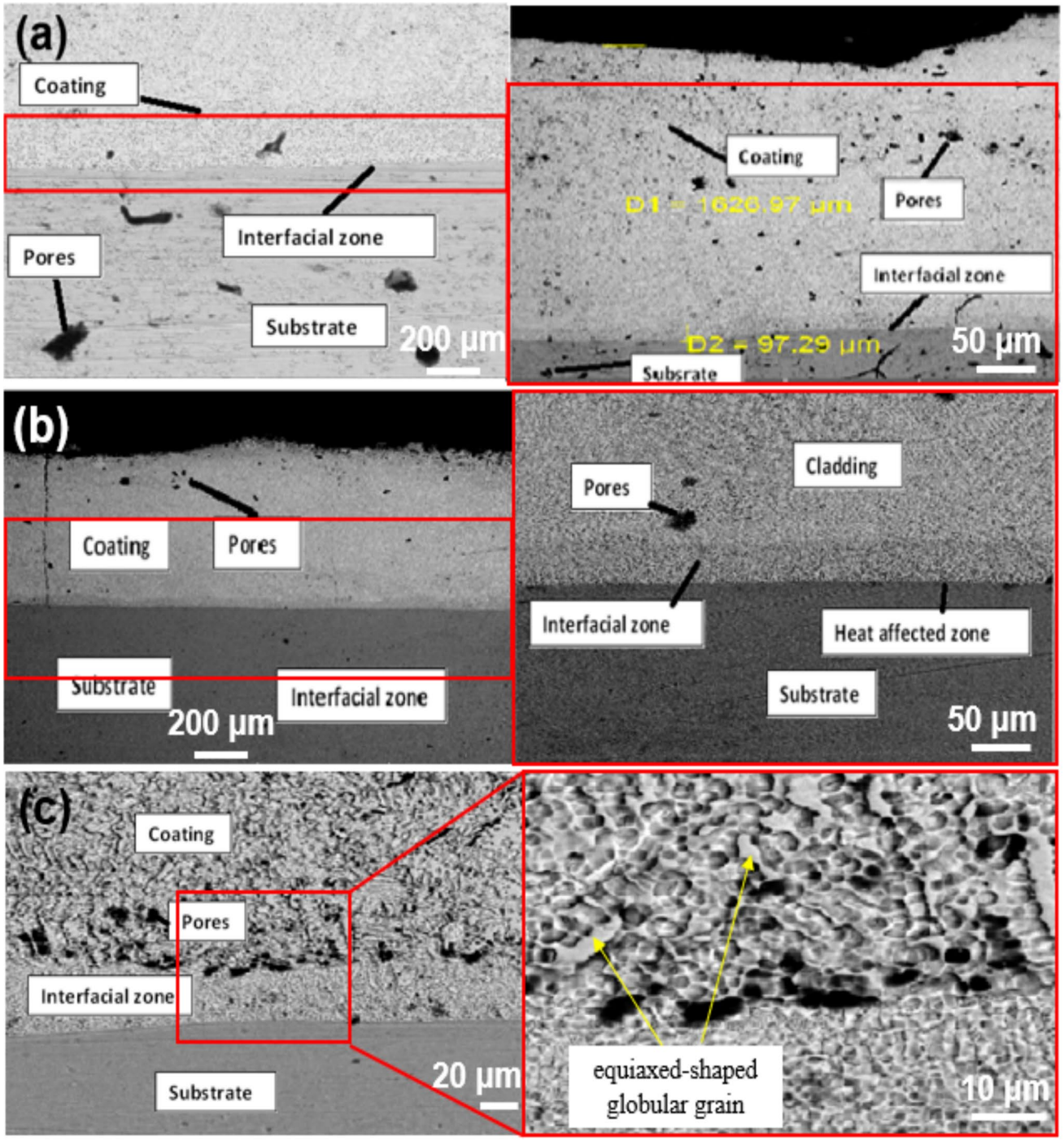

Fig. 5 SEM showing interfacial zone between coatings of 60SiC-20Co-20Ni clad samples at (**a**) 0.4 m/min (**b**) 0.8 m/min (**c**) 1.2 m/min

the strong bond is crucial for the transmission of load and stress between the coating and substrate, thereby enhancing the overall hardness of the composite material. Thus, the highest hardness value observed in coating produced at a laser scanning speed of 1.2 m/min. Similar results were reported by Yu et al [15].

3.4 Corrosion behaviour of coatings in 1 M H_2SO_4

Figure 7 represents the potentiodynamic polarization curves of the substrate and coatings in 1 M H_2SO_4, while Table 3 displays the electrochemical characteristics determined from Tafel line extrapolation, including corrosion

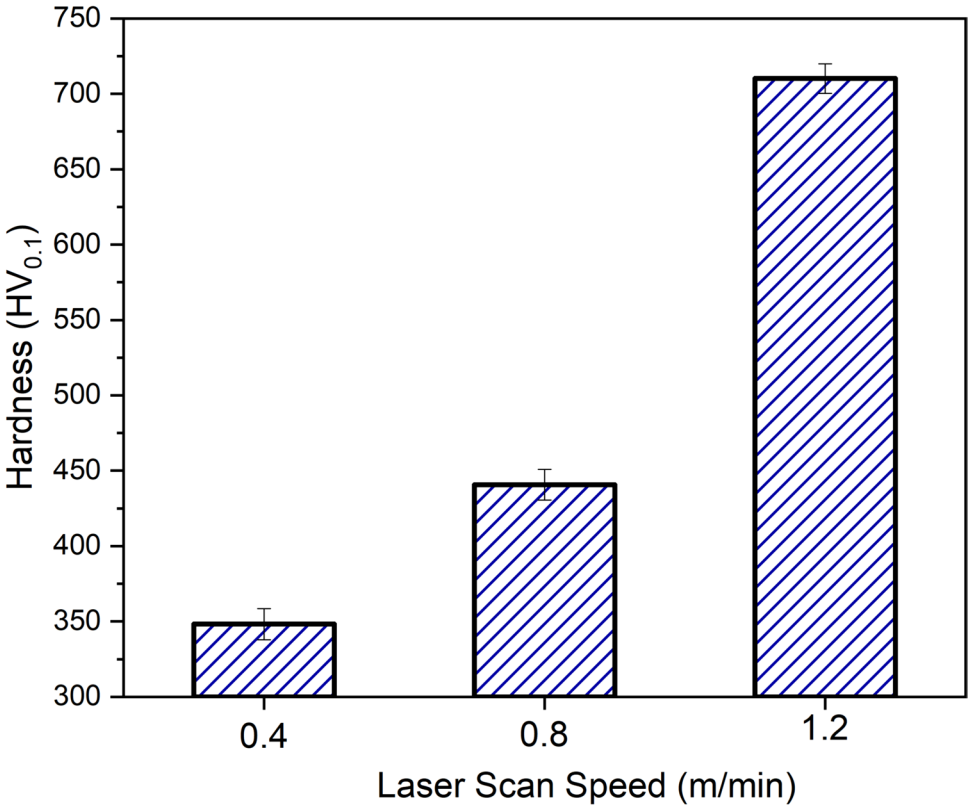

Fig. 6 Micro-hardness of 60SiC-20Co-20Ni cladded layer under various scanning speeds

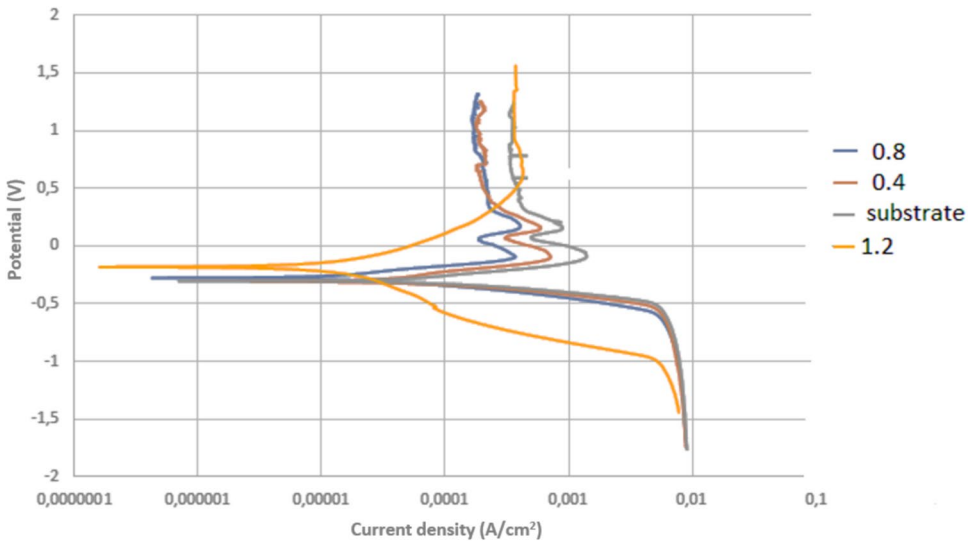

Fig. 7 Polarization curves of laser deposited 60SiC-20Co-20Ni ternary coating with substrate in 1 M sulphuric acid

Table 3 Corrosion test data for 60SiC-20Co-20Ni ternary coating

Sample	E_{corr}, (V)	I_{corr} (A/cm^2)	Polarization resistance R_p (Ω)	Corrosion rate (mm/year)
Substrate	-0.39	9.5E-03	59.3	0.652
Speed 0.4	-0.30	2.7E-04	118.63	0.023145
Speed 0.8	-0.29	2.2E-04	157.93	0.018905
Speed 1.2	-0.20	9.8E-05	234.88	0.008445

potential, corrosion rate, and corrosion current density. Since a significant potential energy is needed to degrade or corrode the alloy, samples with high corrosion potentials had a lower propensity to do so [36]. High positive potentials are evidence of the sample's surface spontaneously passivating. Figure 7 illustrates that all samples, including the substrate, exhibit a similar trend in both the anodic and cathodic branches (comparable polarization curves), with the exception of the sample produced at a

جامعة قطر QATAR UNIVERSITY

scan speed of 1.2 m/min, which displayed a more noble potential. Additionally, the samples demonstrate fluctuations in the passive region, featuring a significant shift in current (current disruption, i.e., transition from active to passive behaviours) between -0.3 to 0.2 V, followed by a more stable passivation curve. Notably, the active-passive phenomenon was not observed for the sample produced at 1.2 m/min, possibly attributed to phases formed at the faster laser scan speed affecting the surface chemistry in 1 M H_2SO_4.

The corrosion behavior of the coating may also be influenced by the presence of Si, Co, and Ni content. Table 3 reveals that the corrosion current density (Icorr) and corrosion potential (Ecorr) for the sample produced at 1.2 m/min were 9.8×10^{-5} A/cm^2 and -0.2 V, respectively, while the substrate's Icorr and Ecorr were 9.5×10^{-3} A/cm^2 and -0.39 V, respectively. The highest polarization resistance is 234.88 Ω for the coating at a scan speed of 1.2 m/min, and the lowest was found at a speed of 0.4 m/min with a resistance of 118.63 Ω. The polarization resistance of the as-received substrate is 59.3 Ω. There is also a noticeable correlation between scan speed and polarization resistance, indicating that an increase in scanning speed results in higher polarization resistance. The improved corrosion resistance of sample coated at a laser scan speed of 1.2 m/min could be attributed to its fine grain size as shown Fig. 4c. Finer grains possess a higher density of grain boundaries and promotes formation of homogeneous and continuous layer of passive oxides, which act as barriers to the diffusion of the corrosive species, consequently hindering the propensity for severe corrosion. This aligns with the findings of Adesina et al. [5], who reported an increase in corrosion resistance of ternary coating on Ti-6Al-4V at a laser scanning speed of 1.2 m/min. In summary, the corrosion response of all coatings is contingent on the laser processing parameters.

3.5 Phase (XRD) analysis after corrosion attach in 1 M of sulphuric acid

Figure 8 illustrates the phases present in 60SiC-20Co-20Ni ternary coatings after corrosion in 1 M H_2SO_4 solution with respect to the varying scanning speed. The diffraction spectrum of the cladded samples shows the presence of protective oxide layers such as TiO, NiO, and SiO after the corrosion attack on the samples. NiO protective oxide is observed to increase in phase intensity as the scanning speed increases, this is an indication that the presence of nickel in the admixed powder played an important role in reducing the corrosion rate of the cladded samples as seen in Fig. 7. An important observation to make is that, regardless of the varying laser scanning speeds, titanium oxide (TiO) consistently dominated the

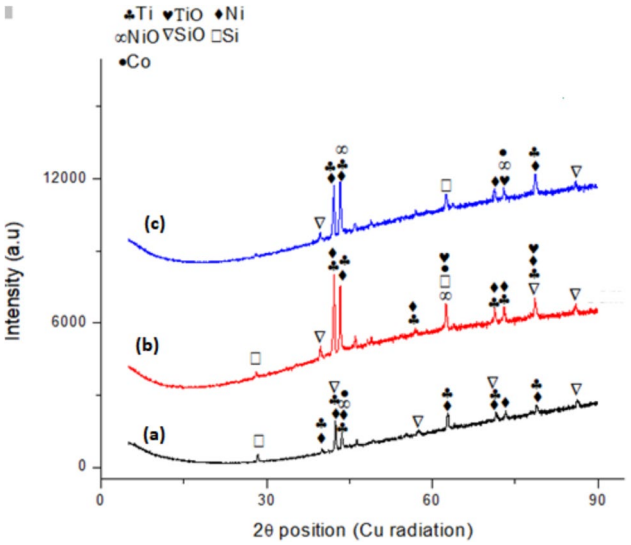

Fig. 8 XRD spectrum of 60SiC-20Co-20Ni coating after corrosion attack of sample (a) I (0.6 m/min) (b) J (0.8 m/min) (c) K (1.2 m/min)

composition of all the coatings. This serves as evidence that the energy density delivered by the laser beam in this study was sufficient to induce the melting of the substrate material, leading to the release of Titanium oxide from the substrate itself. In essence, the preeminent constituents across the coatings, as evident in the phase peak presented in Fig. 8c, are titanium, nickel, and their corresponding protective oxides (TiO and NiO). This prevalence can be attributed to the exceptional shielding properties, stability, corrosion resistance in aggressive environments, and high catalytic activity exhibited by these elements in various electrochemical processes. In support of this, Ibrahim et al [37] reported that NiO serves as a robust reinforcing material with remarkable corrosion resistance attributes. Furthermore, according to Prando et al [38], titanium boasts exceptional corrosion resistance due to its capacity to form an innate exterior oxide layer that acts as a protective barrier.

Based on the polarization analysis, it becomes evident that the 60SiC-20Co-20Ni ternary coating, deposited on Ti-6Al-4V at a laser speed of 1.2 m/min, demonstrates the highest polarization resistance. To investigate the impact of this specific laser scanning speed on the corroded surface, an SEM micrograph of this sample was captured. As illustrated in Fig. 9, the micrograph reveals complex surface features, including the presence of oxide layers. Upon closer examination, it is evident that the surface exhibits localized areas of attack, characterized by irregularities and the formation of cracks within the oxide layer. The observed morphology suggests the formation of a non-homogeneous and potentially defective passive oxide film, which may serve as initiation sites for localized

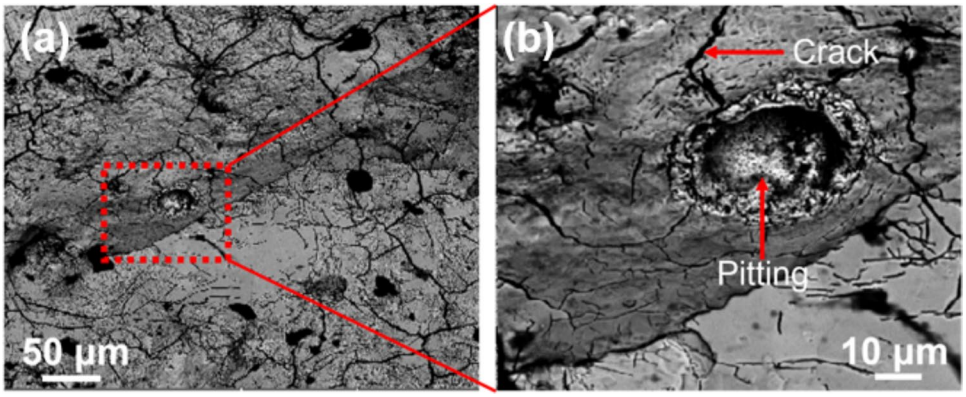

Fig. 9 (**a**) SEM micrograph of the clad sample at a laser speed of 1.2 m/min and (**b**) High magnification image of the selected region in (**a**), after corrosion resistance

dissolution. This phenomenon can be attributed, in part, to the chemical composition and the admixed proportion of the coating alloy. The interaction between the alloy constituents and the corrosive environment likely contributes to the variability in oxide layer morphology and the propensity for localized corrosion. While the surface does exhibit oxide layers, the characterization reveals a complex interplay between surface features and corrosion behavior [39].

The structural phases within Co-Ni coatings encompass FCC for pure nickel, HCP for pure cobalt, and a combination of FCC and HCP phases as the cobalt percentage increases [40, 41]. The collaborative influence of Co-Ni elements, which enhance passivation, contributes to the fortification of passive oxide layers, consequently elevating the coatings' resistance to corrosion. The presence of these protective passive oxides serves as a shield against corrosion attacks, effectively lowering the corrosion rate.

However, in the case of sample K (Fig. 9a), localized pitting corrosion is evident as shown in Fig. 9b. This phenomenon can be attributed, at least in part, to the aggressive nature of the sulfuric acid environment, which leads to the deterioration of passive oxides as the electrochemical current density rises. Pitting corrosion is a form of localized corrosion that can manifest on passivated surfaces due to the impact of environmental factors [42].

Moreover, the appearance of cracks and pitting corrosion in sample K can be attributed to the inherently brittle nature of nickel and the presence of silicon oxide on the surface. Additionally, variations in chemical composition at grain boundaries may have contributed to the observed phenomena, potentially exacerbating the susceptibility to corrosion and mechanical failure in these regions. During corrosion, micro-galvanic passive oxides are formed, which serves as inert physical barriers, inhibiting the initiation of corrosion or the further expansion of corrosion products, particularly in the context of a sulfuric environment after corrosion [39].

4 Conclusion

The present study has effectively integrated SiC-Co-Ni ternary coatings onto the surface of Ti6Al4V through the utilization of the laser cladding technique under varied laser scanning speeds of 0.4, 0. 8, and 1.2 m/min. The following deduction were made from the findings of this work.

- SEM micrographs revealed that increasing laser scan speed leads to reduced laser-materials interaction time and increased solidification rate, resulting in the formation of smaller grains due to insufficient time for grain growth. Therefore, as the laser scanning speed escalates from 0.4 to 0.8 m/min, a finer grain growth pattern emerges. At a laser scanning speed of 1.2 m/min, the solidification process results in the fragmentation of secondary dendrite arms, leading to the formation of equiaxed-like globular grains. This phenomenon is discerned through the appearance of titanium and carbon-rich zones.
- Microhardness analysis indicates a progressive rise in the hardness of the cladded samples as the laser scanning speed increases. Among the samples, sample K produces the most resilient coating, featuring a notable 105.14% augmentation in hardness compared to the substrate. This is attributed to the development of globular grains.
- In terms of electrochemical behavior, the sample denoted as K exhibits the highest polarization resistance (Rp) at 234.88, accompanied by the lowest corrosion rate (Cr) at 0.008445 mm/yr. Thus, for enhancing the corrosion performance of Ti-6Al-4V within an H_2SO_4 environment, the superiority lies with the 60SiC-20Co-20Ni ternary coating at a laser scanning speed of 1.2 m/min.

Authors' contributions This work was carried out in collaboration between all authors. Authors: Olanrewaju Seun Adesina, Abimbola Patricia Popoola, Gabriel Ayokunle Farotade and Babatunde Abiodun Obadele designed the study, performed the experiment, interpreted results and wrote the first draft of the manuscript. Authors, Olufemi Oluseun Sanyaolu, Samson Olaitan Jeje & Azeez Lawan Rominiyi managed the analyses of the study, managed literature searches and graphical editing. All authors read and approved the final manuscript.

Funding Open access funding provided by Tshwane University of Technology.

Data availability All data generated or analyzed during this study are included in this published article.

Declarations

Ethical approval Collection of plant material, comply with relevant institutional, national, and international guidelines and legislation.

Consent to participate Not applicable.

Consent for publication Not applicable.

Competing interests Not applicable.

Open Access This article is licensed under a Creative Commons Attribution 4.0 International License, which permits use, sharing, adaptation, distribution and reproduction in any medium or format, as long as you give appropriate credit to the original author(s) and the source, provide a link to the Creative Commons licence, and indicate if changes were made. The images or other third party material in this article are included in the article's Creative Commons licence, unless indicated otherwise in a credit line to the material. If material is not included in the article's Creative Commons licence and your intended use is not permitted by statutory regulation or exceeds the permitted use, you will need to obtain permission directly from the copyright holder. To view a copy of this licence, visit http://creativecommons.org/licenses/by/4.0/.

References

1. B.A. Obadele, O.O. Ige, P.A. Olubambi, Fabrication and characterization of titanium-nickel-zirconia matrix composites prepared by spark plasma sintering. J. Alloys Compd. **710**, 825–830 (2017)
2. S. Feng, H. Tang, S. Zhang, H. Wang, Microstructure and wear resistance of laser clad TiB–TiC/TiNi–Ti2Ni intermetallic coating on titanium alloy. Trans. Nonferrous Metals Soc. China **22**(7), 1667–1673 (2012)
3. J.D. Majumdar, I. Manna, in *Laser Surface Engineering*. Laser surface engineering of titanium and its alloys for improved wear, corrosion and high-temperature oxidation resistance (Elsevier, 2015), pp. 483–521
4. O.S. Fatoba, O.S. Adesina, A.P.I. Popoola, Evaluation of microstructure, microhardness, and electrochemical properties of laser-deposited Ti-Co coatings on Ti-6Al-4V Alloy. Int. J. Adv. Manuf. Technol. **97**, 2341–2350 (2018)
5. O.S. Adesina et al., Influence of phase composition and microstructure on corrosion behavior of laser based Ti–Co–Ni ternary coatings on Ti–6Al–4V alloy. J. Alloys Compd. **827**, 154245 (2020)
6. F. Contu, B. Elsener, H. Böhni, Serum effect on the electrochemical behaviour of titanium, Ti6Al4V and Ti6Al7Nb alloys in sulphuric acid and sodium hydroxide. Corros. Sci. **46**(9), 2241–2254 (2004)
7. V. Oliveira, C. Aguiar, A. Vazquez, A. Robin, M.J.R.J.C.S. Barboza, Improving corrosion resistance of Ti–6Al–4V alloy through plasma-assisted PVD deposited nitride coatings. Corros. Sci. **88**, 317–327 (2014)
8. O. Adesina, G. Farotade, A.J.M.R.E. Popoola, Synthesis, parametric and tribological study of laser clad Co–Ni binary coatings on titanium alloy. Materials Research Express **6**(5), 056512 (2019)
9. H. R. Tiyyagura and K. C. Kumar, "Investigation on Electro-Chemical Beh H2SO4 and HCl Solutions," 2017.
10. H. Paydas, A. Mertens, R. Carrus, J. Lecomte-Beckers, J.T. Tchuindjang, Laser cladding as repair technology for Ti–6Al–4V alloy: Influence of building strategy on microstructure and hardness. Mater. Des. **85**, 497–510 (2015)
11. Y. Cai et al., Influence of dilution rate on the microstructure and properties of FeCrCoNi high-entropy alloy coating. Mater. Des. **142**, 124–137 (2018)
12. D.M. Goodarzi, J. Pekkarinen, A. Salminen, Effect of process parameters in laser cladding on substrate melted areas and the substrate melted shape. J. Laser Appl. **27**(S2) (2015)
13. H. Wang, Y. Cheng, X. Zhang, J. Yang, C. Cao, Effect of laser scanning speed on microstructure and properties of Fe based amorphous/nanocrystalline cladding coatings. Mater. Chem. Phys. **250**, 123091 (2020)
14. W. Tao, Z. Jin, J. Shuai, Y. Fen, Effect of laser scanning and milling speed on surface roughness of TC4 hybrid prepared. Int. J. Adv. Manuf. Technol. **117**(5-6), 1663–1674 (2021)
15. H. Yu, X. Meng, Z. Wang, C.J.M. Chen, Influence of scanning speed on the microstructure and wear resistance of laser alloying coatings on Ti-6Al-4V substrate. Materials **15**(17), 5819 (2022)
16. J. Chen et al., Effect of the scanning speed on microstructural evolution and wear behaviors of laser cladding NiCrBSi composite coatings. Opt. Laser Technol. **72**, 86–99 (2015)
17. O. Adesina, A. Popoola, S.L. Pityana, D.T. Oloruntoba, A study on scan speed relationship with microstructural evolution, phase composition and microhardness of Ni-containing intermetallic coatings on Ti–6Al–4V using laser cladding technique. Surf. Rev. Lett. **25**(08), 1950035 (2018)
18. L. Wang, Y. Gao, Q. Xue, H. Liu, T. Xu, Microstructure and tribological properties of electrodeposited Ni–Co alloy deposits. Appl. Surf. Sci. **242**(3-4), 326–332 (2005)
19. N. Li et al., Microstructure, formation mechanism and property characterization of Ti+ SiC laser cladded coatings on Ti6Al4V alloy. Mater. Charact. **148**, 43–51 (2019)
20. Y. Wang, X.-B. Liu, Y.-F. Liu, Y.-S. Luo, Y.J.C.I. Meng, Microstructure and tribological performance of Ni60-based composite coatings on Ti6Al4V alloy with different Ti3SiC2 ceramic additions by laser cladding. Ceram. Int. **46**(18), 28996–29010 (2020)
21. Y. Liu, M.Q. Li, Structure response characteristics and surface nanocrystallization mechanism of alpha phase in Ti-6Al-4V subjected to high energy shot peening. J. Alloys Compd. **773**, 860–871 (2019)
22. B.A. Obadele, A. Andrews, A. Olubambi, M.T. Mathew, S. Pityana, Effect of ZrO2 addition on the dry sliding wear behavior of laser clad Ti6Al4V alloy. Wear **328**, 295–300 (2015)
23. O.S. Adesina, A.I. Popoola, A study on the influence of laser power on microstructural evolution and tribological functionality of metallic coatings deposited on Ti-6Al-4V alloy. Tribol. - Mater. Surf. Interfaces **11**(3), 145–155 (2017)
24. H. Dong, "3 - Tribological properties of titanium-based alloys," Woodhead Publishing Series in Metals and Surface Engineering, 58-80, 2010.
25. L.U.O. Fang, Y.A.O. Jian-hua, H.U. Xia-xia, C. Guo-zhong, Effect of Laser Power on the Cladding Temperature Field and the Heat Affected Zone. J. Iron Steel Res. Int. **18**(1), 73–78 (2011)

26. Z. Baicheng, D. Lucas, C. Christian, The study of the laser parameters and environment variables effect on mechanical properties of high compact parts elaborated by selective laser melting 316L powder. Mater. Sci. Eng. A **584**, 21–31 (2013)
27. D. Dey, K.S. Bal, A.K. Singh, A.R. Choudhury, Hardness and wear behaviour of multiple component coating on Ti-6Al-4V substrate by laser application. Optik **202**, 163555 (2020)
28. A.V. Adedayo, Development processes of globular microstructure. J. Miner. Mater. Charact. Eng. **10**, 651 (2011)
29. C. Han et al., Nucleation mechanisms of equiaxed grains in the fusion zone of aluminum-lithium alloys by laser welding. J. Mater. Res. Technol. **14**, 2219–2232 (2021)
30. X. Luo et al., Overcoming the strength–ductility trade-off by tailoring grain-boundary metastable Si-containing phase in β-type titanium alloy. J. Mater. Sci. Technol. **68**, 112–123 (2021)
31. R. Chai, Y. Zhang, B. Zhong, C. Zhang, Effect of scan speed on grain and microstructural morphology for laser additive manufacturing of 304 stainless steel. Rev. Adv. Mater. Sci. **60**(1), 744–760 (2021)
32. Q. Li, Y. Lei, H. Fu, Laser cladding in-situ NbC particle reinforced Fe-based composite coatings with rare earth oxide addition. Surf. Coat. Technol. **239**, 102–107 (2014)
33. R. Qin et al., Laser cladding of high Co–Ni secondary hardening steel on 18Cr2Ni4WA steel. Surf. Coat. Technol. **285**, 242–248 (2016)
34. J. Wang, I. Timokhina, K. Sharp, A. Shekhter, Q. Liu, Microstructure and precipitation behaviours of laser clad 7075 aluminium alloy. Surf. Coat. Technol. **445**, 128726 (2022)
35. S.V. Hainsworth, W.C. Soh, The effect of the substrate on the mechanical properties of TiN coatings. Surf. Coat. Technol. **163**, 515–520 (2003)
36. J. Van der Merwe, D. Tharandt, Corrosion resistance of laser-cladded 304L stainless steel enriched with ruthenium additions exposed to sulphuric acid and sodium chloride media. J. South. Afr. Inst. Min. Metall. **115**(6), 499–505 (2015)
37. M. Ibrahim et al., "Enhanced corrosion protection of epoxy/ZnO-NiO nanocomposite coatings on steel," Coatings 10, 8, 783, 2020.
38. D. Prando et al., Corrosion of titanium: Part 1: Aggressive environments and main forms of degradation. J. Appl. Biomater. Functional Mater. **15**(4), e291–e302 (2017)
39. B. Bakhit, A. Akbari, F. Nasirpouri, M.G.J.A.S.S. Hosseini, Corrosion resistance of Ni–Co alloy and Ni–Co/SiC nanocomposite coatings electrodeposited by sediment codeposition technique. Appl. Surf. Sci. **307**, 351–359 (2014)
40. B. Fatima Zohra, N. Abderrafik, M. Hayet, R. Jean Luc, Morphology and Rietveld analysis of nanostructured Co-Ni electrodeposited thin films obtained at different current densities. Surf. Coat. Technol. **315**, 172–180 (2017)
41. K. Sharifi, M. Ghorbani, Corrosion Behaviour of Ni–Co Alloy Coatings at Kish Island (Marine) Atmosphere. Bull. Mater. Sci. **37**(3), 713–719 (2014)
42. B. Gerd, in Supercritical Fluid Science and Technology. Chapter 12 - Corrosion in Hydrothermal and Supercritical Water. (5), 591–619 (Elsevier, 2014)